

Evaluation of the phase randomness of the light source in quantum key distribution systems with an attenuated laser

Toshiya Kobayashi,* Akihisa Tomita, and Atsushi Okamoto

Graduate School of Information Science and Technology, Hokkaido University

Kita 14, Nishi 9, Sapporo 060-0814, Japan

Abstract

The phase randomized light is one of the key assumptions in the security proof of Bennett-Brassard 1984 (BB84) quantum key distribution (QKD) protocol implemented with an attenuated laser. Though the assumption has been believed to be satisfied for conventional systems, it should be reexamined for current high speed QKD systems. The phase correlation may be induced by the overlap of the optical pulses, the interval of which decreases as the clock frequency. The phase randomness was investigated experimentally by measuring the visibility of interference. An asymmetric Mach-Zehnder interferometer was used to observe the interference between adjacent pulses from a gain-switched distributed feedback laser diode driven at 10 GHz. Low visibility was observed when the minimum drive current was set far below the threshold, while the interference emerged when the minimum drive current was close to the threshold. Theoretical evaluation on the impact of the imperfect phase randomization provides target values for the visibility to guarantee the phase randomness. The experimental and theoretical results show that secure implementation of decoy BB84 protocol is achievable even for the 10-GHz clock frequency, by using the laser diode under proper operating conditions.

* Present address: Seiko Epson Corporation

I. INTRODUCTION

Quantum key distribution (QKD) offers an unconditionally secure method to share a cryptographic key between remote parties. Bennett-Brassard 1984 (BB84) protocol [1] is one of the most developed QKD protocols, the security proof of which has been well established [2–5]. Recent researches on the security focus on more practical aspects, such as imperfections in a QKD apparatus. In actual QKD equipment, the device characteristics deviate from the ideal ones. Keeping the secure key rate with imperfect devices is an important issue [6, 7]. Since a practical single photon source, assumed in the original BB84 protocol, is still unavailable, most QKD experiments have utilized light pulses from a laser diode (LD) after strong attenuation. The attenuated laser pulses contain two photons or more with a finite probability. The multiple photon states opened the way to an efficient eavesdropping method called photon number splitting (PNS) attack [8]. Gottesman, Lo, Lütkenhaus, and Preskill (GLLP [9]) analyzed the security against this imperfection. An improved protocol called decoy-BB84 [10–12] was proposed to yield better secure key rate than GLLP. The decoy-BB84 protocol provides not only unconditional security with the attenuated laser light, but also the universal composability [13–16].

The strongly attenuated laser light is often called weak coherent light. This term is misleading, because the security analysis in the GLLP and decoy-BB84 articles assumes that the light source emits photons in a phase randomized Poissonian state, which is a mixture of coherent states with uniformly distributed phases:

$$\rho = \frac{1}{2\pi} \int_{-\pi}^{\pi} d\phi |\alpha e^{i\phi}\rangle \langle \alpha e^{i\phi}| = e^{-|\alpha|^2} \sum_{n=0}^{\infty} \frac{\alpha^{2n}}{n!} |n\rangle \langle n|. \quad (1)$$

The state is represented by a diagonal density matrix with respect to photon-number basis. Lo and Preskill [17] showed that, if the photon states were really weak coherent, discrimination of the bases used in the BB84 protocol would be easier. Recently, Tang, et al. [18] showed that the phase information also increases distinguishability between decoy and signal pulses used in the decoy-BB84 protocol. Those reports have issued a warning about the phase correlation among the laser pulses; the phase correlation will increase the information leakage and thus reduce the secure key rate. Active phase randomization was proposed and implemented by Zhao, et al. [19]. Effect of partially randomized phase was also examined for a plug-and-play system [20].

Nevertheless, most experimentalists have not taken this warning seriously with a few exceptions [18–20]. Their common belief is that pulses from a gain-switched LD have no phase relationship to other pulses. Therefore, the phase of the light source is automatically randomized, as long as the one-way QKD architecture is employed. The mechanism of the phase randomization is following. In the gain-switched mode, each current pulse excites the semiconductor medium from loss to gain. A laser pulse is generated from seed photons originated from spontaneous emission, because the photons from the previous lasing have vanished during the pulse interval. The phase of the spontaneous emission is random, so that the phase of the laser pulses should vary from one pulse to another. This is true when the previously lased photons disappear completely in the interval. However, if the photons survive until the next excitation, the lasing can be seeded by the remaining photons. Then, the phase of the laser pulse may relate to the previous one, because the stimulated emission conserves the phase. The effect of the residual photons will emerge significantly by increasing the pulse repetition rate and narrowing the pulse interval. The state-of-art QKD systems operate at high clock frequencies over 1 GHz, along with the improvement of the photon detectors [21–23]. The clock frequency would further increase to meet demands for high bit-rate secure communication. The interval time thus decreases down to hundreds picoseconds or even shorter. Furthermore, the drive current may not return to zero in order to improve modulation response of the laser. It is unclear whether the assumption of the phase randomized source still holds in QKD systems operated at several GHz-clock frequencies.

In this article, we examine the phase randomness of the light source at 10-GHz clock frequency. Sec. II A introduces an asymmetric interferometer set-up to measure the phase correlation between the adjacent optical pulses. We recall the relation of the phase correlation to the visibility of the interference fringe. Sec. II B considers the effects of the partial coherence in state discrimination, which were analyzed by Lo-Preskill [17] and Tang et al. [18] for perfectly coherent states. We provide target values of the visibility, under which we can regard the light source as phase randomized. Sec. III shows the measured visibility of the interference fringe of the adjacent pulses from a LD operated at 10-GHz clock frequency. We controlled DC bias current to the LD, which determines the effective pulse interval and the minimum drive current. In sec. IV, we examine the accuracy of the estimated values of visibility, and applied corrections to the estimation. We investigate the relation between the

observed phase correlation and the operating conditions, in terms of the effective photon life time of the LDs.

II. THEORY

A. Relation between visibility and phase correlation

The phase relation of laser light can be characterized with an interferometer. Figure 1 illustrates a schematic of an asymmetric interferometer to observe interference between the adjacent optical pulses. We focus on measuring the interference between the adjacent pulses, because the phases between the adjacent pulses are more correlated than those between more temporally-separated pulses. Light pulses generated in the source enter the asymmetric interferometer, where the delay time is adjusted to the pulse period. The adjacent optical pulses are combined at the output. A phase modulator is placed in one arm of the interferometer to provide a phase difference φ between the paths. The signals are detected by a high-speed photodetector and accumulated by an averager. If a fixed phase relation between the adjacent pulses exists, the amplitude of the signal takes a definite value according to the phase difference between the optical paths. A clear interference fringe will be observed as φ varies. If the phases between the pulses are random, the interference signal differs from pulse to pulse. Then the interference fringe will disappear after accumulation. Visibility of interference Θ , which represents the degree of the phase correlation, is defined by

$$0 \leq \Theta := \frac{I_{max} - I_{min}}{I_{max} + I_{min}} \leq 1, \quad (2)$$

where I_{max} and I_{min} stand for the peak (maximum) and the valley (minimum) of the interference fringe, respectively. As the phase correlation becomes stronger, the visibility gets closer to one.

In the following, we recall a relation between the visibility and the phase correlation [24]. The output intensity of the interferometer is given by

$$I(\varphi) \propto \mathcal{E}^2 \{ |a_A|^2 + |a_B|^2 + |a_A a_B| \exp[i(\theta + \varphi)] + \text{c.c.} \}, \quad (3)$$

where the coefficient $\mathcal{E} = \sqrt{\hbar\omega/2\epsilon_0 V}$ carries the dimension of electric field. The complex amplitudes a_A and a_B represent the fields provided from paths A and B , respectively. In

the asymmetric interferometer, the fields a_A and a_B correspond to those of the adjacent pulses. The relative phase between the pulses is given by θ . The third and forth terms of Eq. (3) are responsible for the interference. Taking an average over an ensemble, we obtain the interference terms as

$$\langle a_A a_B \rangle \langle e^{i\theta} \rangle e^{i\varphi} + \text{c.c.}, \quad (4)$$

where we assume the phase difference φ varies slowly, while the relative phase θ is a probabilistic variable. Equation (4) shows that the interference visibility is governed by the expectation value of the relative phase $\langle e^{i\theta} \rangle$. If the distribution of the phase obeys a Gaussian probability density function with the central value θ_0 and the standard deviation σ

$$g(\theta, \theta_0) = \frac{1}{\sqrt{2\pi\sigma^2}} \exp \left[-\frac{(\theta - \theta_0)^2}{2\sigma^2} \right], \quad (5)$$

the expectation value is given by

$$\begin{aligned} \langle e^{i\theta} \rangle &= \int_{-\infty}^{\infty} e^{i\theta} g(\theta, \theta_0) d(\theta) \\ &= \exp \left[-\frac{\sigma^2}{2} + i\theta_0 \right]. \end{aligned} \quad (6)$$

The Gaussian probability distribution describes the phase distribution of the LD light well, because the light field vector (phaser) in the phase space is kicked by a number of photons generated by spontaneous emission [25]. The kicks force the field vector to walk randomly around the original position. Since the spontaneous emission occurs independently, a number of kicks results in the Gaussian distribution. Using Eqs. (2)-(6), we relate the visibility to the standard deviation of the phase distribution as

$$\Theta = \exp \left[-\frac{\sigma^2}{2} \right]. \quad (7)$$

Here, we assume $|a_A| = |a_B|$ for simplicity. As expected, the visibility decreases rapidly with increasing the standard deviation of the phase. The analysis given above uses the classical complex amplitude of the electric field, because the laser field can be well approximated with a classical field, where the effect of the spontaneous emission is introduced by a random kick [24, 25]. The wave properties of the field will not be altered by attenuation. Furthermore, the analysis using quantum operators will provide the similar description.

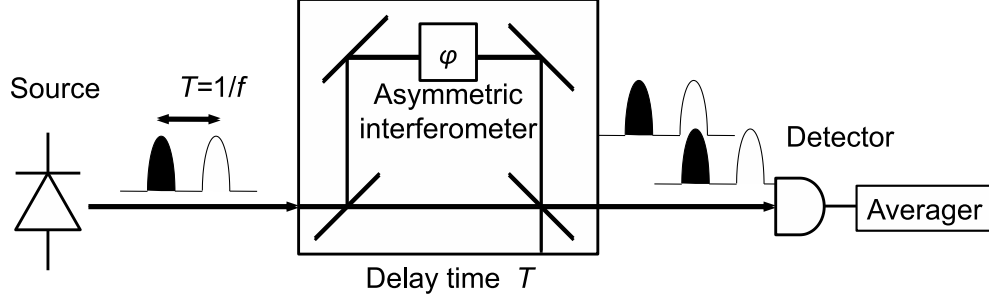


FIG. 1. A schematic illustration of a measurement apparatus for the phase correlation between the adjacent pulses. The delay time of the asymmetric interferometer is adjusted to the pulse period. The phase difference φ between the paths can be modulated.

B. Impact of phase correlation

We consider the impact of phase correlation to provide criteria to guarantee the security of decoy-BB84 with a LD light source. As stated in the introduction, the phase correlation enhances the distinguishability of the states, which are expected to be indistinguishable in the ideal situation [17, 18]. The following calculation will treat two issues on the state discrimination: one is between the states of different bases, and the other is between the signal and decoy pulses.

Most security proofs of BB84 rely on the assumption that the density matrix of one basis is indistinguishable to another. The distinguishability of two density matrices, sometimes called the imbalance of the quantum coin [9], helps the eavesdropper (Eve) to distinguish the state encoding. GLLP [9] described the imbalance in terms of the fidelity between the density matrices, and analyzed its effects on the security. Though the imbalance of the quantum coin often refers to the state preparation flaws, Lo and Preskill [17] showed that phase correlation also enhances the distinguishability. The imbalance of the quantum coin Δ is given by

$$\Delta = \frac{1 - F(\rho_X, \rho_Z)}{2}, \quad (8)$$

where the fidelity of the density matrices in X -coding and Z -coding is defined by

$$F(\rho_X, \rho_Z) = \text{Tr} \left(\rho_Z^{1/2} \rho_X \rho_Z^{1/2} \right)^{1/2}. \quad (9)$$

Further, since Eve may exploit the channel loss, we should recalculate the imbalance to keep

security as

$$\Delta' = \frac{\Delta}{\eta\mu} \quad (10)$$

for given transmittance of the channel η and the average photon number μ of the source. Recently, Tamaki, et al. [26] showed that GLLP analysis was too conservative, and proposed a loss-tolerant proof even with state preparation flaws. We here calculate Δ , because it still provides a comprehensive measure of the state distinguishability. We can obtain Δ' from Δ by Eq. (10), if we follow the GLLP analysis. The density matrices of the partially phase randomized coherent states are expressed by

$$\begin{aligned} \rho_Z &= \frac{1}{2} \int (|\sqrt{\mu}e^{i\theta}\rangle_F \langle\sqrt{\mu}e^{i\theta}| \otimes |0\rangle_S \langle 0| + |0\rangle_F \langle 0| \otimes |\sqrt{\mu}e^{i\theta}\rangle_S \langle\sqrt{\mu}e^{i\theta}|) g(\theta, \theta_0) d\theta \\ &= \frac{1}{2} e^{-\mu} \left(\sum_{M,N} \frac{\mu^{(M+N)/2} e^{-(M-N)^2\sigma^2/2} e^{i(M-N)\theta_0}}{\sqrt{M!N!}} |M\rangle_F \langle N| \otimes |0\rangle_S \langle 0| \right. \\ &\quad \left. + |0\rangle_F \langle 0| \otimes \sum_{M,N} \frac{\mu^{(M+N)/2} e^{-(M-N)^2\sigma^2/2} e^{i(M-N)\theta_0}}{\sqrt{M!N!}} |M\rangle_S \langle N| \right) \end{aligned} \quad (11)$$

$$\begin{aligned} \rho_X &= \frac{1}{2} \int \left(\left| \sqrt{\frac{\mu}{2}} e^{i\theta} \right\rangle_F \left\langle \sqrt{\frac{\mu}{2}} e^{i\theta} \right| \otimes \left| \sqrt{\frac{\mu}{2}} e^{i\theta} \right\rangle_S \left\langle \sqrt{\frac{\mu}{2}} e^{i\theta} \right| \right. \\ &\quad \left. + \left| \sqrt{\frac{\mu}{2}} e^{i\theta} \right\rangle_F \left\langle \sqrt{\frac{\mu}{2}} e^{i\theta} \right| \otimes \left| -\sqrt{\frac{\mu}{2}} e^{i\theta} \right\rangle_S \left\langle -\sqrt{\frac{\mu}{2}} e^{i\theta} \right| \right) g(\theta, 0) d\theta \\ &= \frac{1}{2} e^{-\mu} \sum_{M,N} \left(\frac{\mu}{2} \right)^{(M+N)/2} e^{-(M-N)^2\sigma^2/2} \\ &\quad \times \sum_{m,n} \frac{1 + (-1)^{m-n}}{\sqrt{(M-m)!m!(N-n)!n!}} |M-m\rangle_F \langle N-n| \otimes |m\rangle_S \langle n|, \end{aligned} \quad (12)$$

where the subscripts F and S denote fast and slow components of the time-bin qubits. A finite value of θ_0 is assumed for Z coding, while it is set to zero for X coding. Since only the relative phase between the two coding affects the distinguishability, this setting will not lose generality. The factor $\exp[-(M-N)^2\sigma^2/2]$ decreases rapidly for large σ , and only the $M=N$ terms survive. In this phase randomized limit, the density matrices (11) and (12) coincide with those of the mixture of M -photon number states after the state preparation.

The imbalance of the quantum coin Δ can be calculated with Eq. (8) and the density matrices (11) and (12). The two states ρ_Z and ρ_X are most distinguishable when the central value of the phase $\theta_0 = \pi$, and least distinguishable when $\theta_0 = 0$. We calculated the fidelity numerically with the density matrices in the photon-number-state basis truncated to a finite photon number N_{max} . We changed the number of bases to check the accuracy

of the calculation. Since the average photon number is small, the results converged rapidly at $N_{max} = 8$. We thus set $N_{max} = 16$ in the following calculation. Figure 2 shows the calculated values of Δ as a function of the standard deviation of the phase distribution σ for the average photon numbers μ of 0.09 and 0.01. The imbalance of the quantum coin decreases as the standard deviation. For a small standard deviation, that is, less phase randomized, the imbalance of the quantum coin for $\theta_0 = \pi$ is larger than that for $\theta_0 = 0$. The effect of the central phase difference vanishes for large standard deviation, as the phases of the states become randomized. As seen in Fig. 2, Δ converges to finite values for large standard deviation. The relative errors from the asymptotic values fall below 10^{-2} , when the standard deviation exceeds the following values: 2.9 for $\mu = 0.01$ and $\theta_0 = 0$, 2.6 for $\mu = 0.01$ and $\theta_0 = \pi$, 3.2 for $\mu = 0.09$ and $\theta_0 = 0$, and 2.9 for $\mu = 0.09$ and $\theta_0 = \pi$. The values of standard deviation, 2.6, 2.9, and 3.2, correspond to the visibility of 0.034, 0.015, and 0.006, respectively, which are estimated with Eq. (7). Therefore, target visibility values would be 0.015 for $\mu = 0.01$ and 0.006 for $\mu = 0.09$ in terms of the imbalance of the quantum coin. The asymptotic value of Δ for $\mu = 0.09$ is larger than that for $\mu = 0.01$, due to the multiple photon contribution, which increases the distinguishability between the two states.

Decoy method uses the states with different average photon numbers, called signal and decoy. A key assumption of the decoy method is that Eve cannot distinguish the signal pulses from the decoy. In other words, Eve can measure the photon number contained in a pulse, but cannot measure the average photon number of an individual pulse. Then Eve's strategy is limited to the one that depends on the photon number of the pulse. The security proof of the decoy method only needs to consider such limited eavesdropping strategy. Tang, et al. [18] pointed out that phase correlation enables an unambiguous-state-discrimination (USD) measurement to distinguish the signal from the decoy. The final key generated by the non-phase-randomized system can be compromised by combining the USD measurement and the PNS attack. When the phase is partially randomized, the USD measurement is no longer possible. However, if Eve allows finite probability to obtain inconclusive results P_{inc} , she can still increase the probability of the correct decision P_C [27]. In the appendix, we derive the optimum positive-operator valued measure (POVM) to discriminate the signal state from the decoy state for partially coherent states. The results of the POVM enable to extend the analysis presented by Tang, et al. [18].

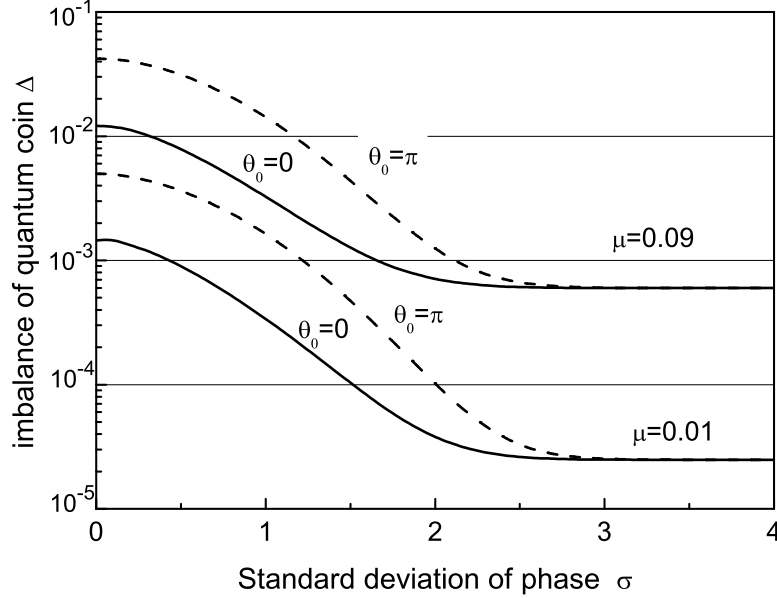


FIG. 2. The imbalance of the quantum coin, defined by $\Delta = (1 - F(\rho_Z, \rho_X))/2$, as a function of standard deviation of phase distribution. Solid lines represent Δ for the difference of central phase value $\theta_0 = 0$, broken lines for $\theta_0 = \pi$.

We investigate the fidelity between the signal and decoy states described by

$$\rho_1 = e^{-a_1^2} \sum_{m,n} \frac{a_1^{m+n} e^{-(m-n)^2 \sigma^2 / 2} e^{i(m-n)\theta_0}}{\sqrt{m!n!}} |m\rangle \langle n| \quad (13)$$

$$\rho_2 = e^{-a_2^2} \sum_{m,n} \frac{a_2^{m+n} e^{-(m-n)^2 \sigma^2 / 2}}{\sqrt{m!n!}} |m\rangle \langle n|. \quad (14)$$

Following Tang, et al. [18], we consider only the fast component of the time-bin qubits, which carries no information on the key bit value. The density matrices ρ_1 and ρ_2 describe partially phase randomized coherent states with the average photon numbers $\mu = 2a_1^2$ and $\nu = 2a_2^2$, respectively. We calculated the fidelity numerically by truncating the number of basis to a finite photon number $N_{max} = 16$, as the imbalance of the quantum coin. Figure 3 shows the distinguishability defined by $(1 - F(\rho_1, \rho_2))/2$ with the fidelity of ρ_1 and ρ_2 . The distinguishability decreases as the phase randomization, and asymptotically reaches the value for the completely phase randomized states. The relative discrepancy between the two became less than 10^{-2} for $\sigma > 2.5$, which corresponds to the visibility of 0.044. This value would be a target visibility in terms of the signal-decoy discrimination. The fidelity was

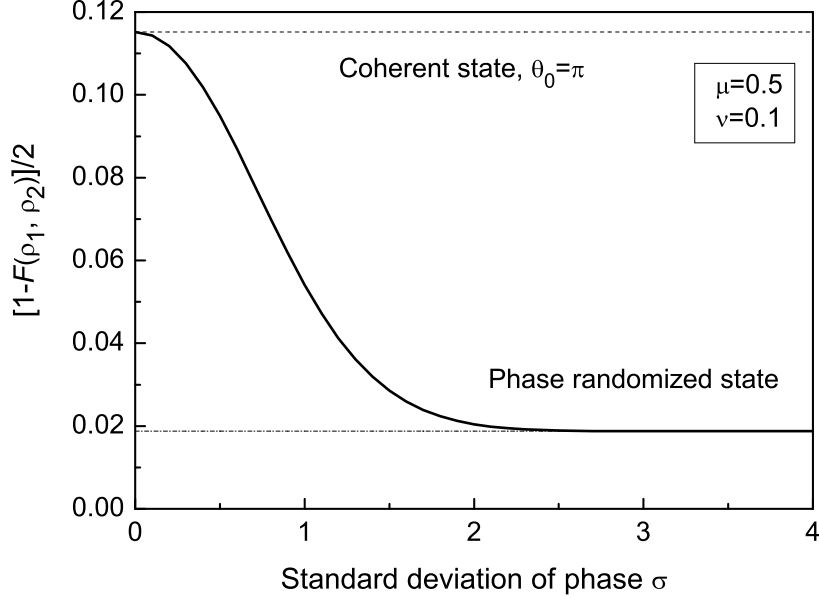


FIG. 3. Distinguishability $(1 - F(\rho_1, \rho_2))/2$ between the signal and decoy states as a function of the standard deviation of phase. Calculation was done for the partially phase randomized states of average photon number 0.5 (signal) and 0.1 (decoy.) Solid line represents the calculated fidelity for $\theta_0 = \pi$. Dash-dot line stands for the distinguishability between the completely phase randomized states, and dash line between coherent states with $\theta_0 = \pi$.

calculated for $\theta_0 = \pi$, because the coherent states with the relative phase $\theta_0 = 0$ yield the same fidelity as the completely phase randomized states. However, the coherent states still provide an advantage to the eavesdropper to perform an individual attack as seen in the appendix.

In this section, we have derived criteria of the phase randomness and thus the interference visibility. The target values depend on the average photon numbers. Moreover, the eavesdropping methods are not exhausted with those considered above, so that the target values may be further lowered. Nevertheless, we believe that the present analysis covers a wide range of eavesdropping, and the values estimated here should be good indications.

III. EXPERIMENT

The phase correlation measurement system consists of the interferometer and the pulsed light source to be tested. We employed the configuration similar to the one depicted in Fig. 1. The source was a distributed feedback (DFB) LD (NEL, NLK5C5EBKA,) which was designed for 10-GHz direct modulation to emit optical pulses in a single longitudinal and transversal mode. It lases around the wavelength of 1560 nm at the threshold current of 9.5 mA. The LD was driven by the combination of a 10-GHz sinusoidal current (I_{AC}) and a DC bias current (I_{DC} .) The total current to the LD is expressed by $I_{AC} + I_{DC}$. The sinusoidal current injected to the laser is expressed by

$$I_{AC} = \frac{I_{pp}}{2} \cos(2\pi ft + \phi_{LD}), \quad (15)$$

where I_{pp} stands for the peak-to-peak value of the sinusoidal current. The current changes periodically with the frequency $f = 10$ GHz and an initial phase ϕ_{LD} . The sinusoidal signal from a pulse-pattern-generator (PPG) was amplified to a fixed amplitude $V_{pp}=4.615$ V. We estimated the peak-to-peak AC current to the LD as $I_{pp}=92.3$ mA, considering the 50- Ω road resistance. However, in high frequency region such as 10 GHz, the emerging effects of parasitic impedances of the LD and the circuit may reduce the current injected into the LD active layer. To correct this effect, we measured the modulation response of the LD with a network analyzer and a 45-GHz band-width photodetector. The resonant-like frequency was about 12 GHz in this measurement, so that the intrinsic response of the LD affects little the modulation response up to 10 GHz. It was found that the optical power response of the LD decreased by about 1 dB at 10 GHz from that at 100 MHz. Since the optical power is proportional to the injected current, we regard the reduction of the response as the decrease of the current with the same proportion. Then the net current I_{net} is reduced from the nominal value I_{nom} by $10 \log_{10} (I_{net}/I_{nom}) = -1$. The net AC current thus swung by $I_{pp} = 92.3 \times 0.794 = 73.3$ mA, where $10^{-1/10} \simeq 0.794$.

The operating condition of the LD was controlled by changing the DC bias current I_{DC} . We define the minimum drive current defined by $I_{min} = -I_{pp}/2 + I_{DC}$, which refers to the drive current at the bottom of the AC current. In the following, we use normalized excitation to describe the operating condition. The normalized minimum excitation is defined by

$$\Lambda = \frac{I_{min} - I_{th}}{I_{th}}. \quad (16)$$

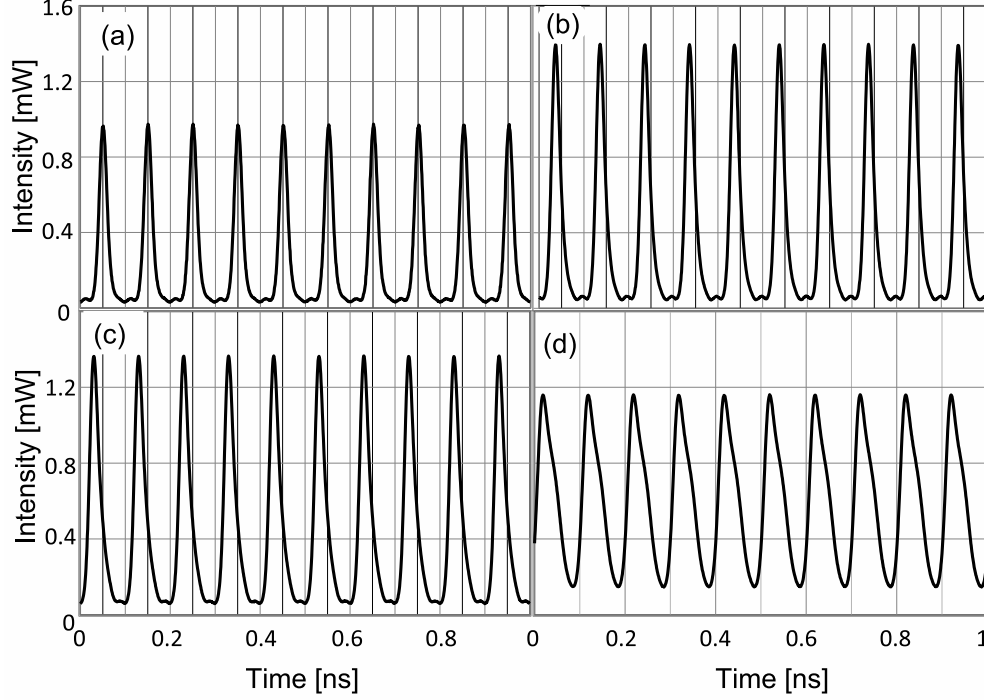


FIG. 4. Waveforms of the LD pulses. The values of the normalized minimum excitation are as follows: (a) $\Lambda = -1.6$, (b) $\Lambda = 0.074$, (c) $\Lambda = 0.49$, and (d) $\Lambda = 2.6$.

As mentioned, the laser threshold current was $I_{th} = 9.5$ mA. When $\Lambda > 0$, the LD was always turned on. When $\Lambda < 0$, the LD was turned off during the pulse interval. The turn-off duration increases as the DC bias current decreases, which is obtained as a solution of $I_{AC} + I_{DC} = I_{th}$ with Eq. (15). When $\Lambda < -1$, the LD was reversely biased and no current was injected at the minimum. In the present experiment, $\Lambda = 0$ and $\Lambda = -1$ correspond to $I_{DC} = 46.15$ mA and $I_{DC} = 36.75$ mA, respectively.

We employed a commercially available asymmetric Mach-Zehnder interferometer (AMZI) module (Kyria, WT-MINT-M-L) to obtain interference between the adjacent pulses at 10 GHz, which was developed as a demodulator for 10-GHz differential phase shift keying (DPSK.) The phase difference between the optical paths was modulated with a phase shifter integrated in the AMZI module. The signal was accumulated for 256 samples and measured with a sampling oscilloscope of 40-GHz optical band-width to observe the interference fringe. The output of the AMZI was attenuated by an optical attenuator to avoid saturation of the photodetector. The peak and valley intensities of the accumulated interference fringes were recorded.

Figure 4 shows the observed waveforms of light pulses for (a) $\Lambda = -1.6$, (b) $\Lambda = 0.074$, (c) $\Lambda = 0.49$, and (d) $\Lambda = 2.6$, where the minimum drive current I_{min} was (a) below the threshold, (b) near the threshold, (c) above the threshold, and (d) far above the threshold. By setting the I_{min} close to the threshold, sharp and intense pulses were obtained as shown in Fig. 4 (b) and (c). When the I_{min} was far above the threshold, the laser output reflected the input current waveform as in Fig. 4 (d). The LD was no longer operated in the gain-switched mode in this DC bias region.

The observed interference fringes are shown in Fig. 5. Clear interference fringe was observed for a large excitation ($\Lambda = 2.6$) with the visibility close to unity ($\Theta = 0.93$), while no clear interference fringe was observed for a small excitation ($\Lambda = -1.6$.) The results indicate that the phases of the pulses for a gain-switched LD are still random even at 10 GHz pulse frequency for a small minimum drive current. In Fig. 5, we plotted the normalized values of the output signal to set the averaged value to 0.5; (Intensity) = (Observed power)/(Averaged Power). Due to the limitation of the device, the range of phase modulation was only slightly larger than 2π . The phase difference of the interferometer was stable enough for the short time to obtain an interference fringe. It was not stable for days, so that the origin of the phase difference varied as shown in Fig. 5(a)-(d.)

IV. DISCUSSION

We consider the origins of errors to examine the accuracy of the results obtained in the experiment. First, the imperfections in the interferometer, such as fluctuation of path length, imbalanced branch ratio of the beam splitters, polarization rotation, and depolarization will reduce the visibility. In fact, we obtained the visibility of only 0.95 with continuous wave (CW) light emitted from the LD excited solely by the DC current of 50 mA, which was far above the threshold. The LD linewidth implies that the phase of the CW light should be well conserved in the time scale of 100 ps. Therefore, we should consider the obtained visibility was affected mainly by the imperfections in the interferometer. Assuming the imperfections are the same throughout the experiment, we should correct the visibility by multiplying 1.05.

Second, the system noise affects the visibility estimation. In the present experiment, we recorded the observed maximum and minimum values, which included noise. Thus, the

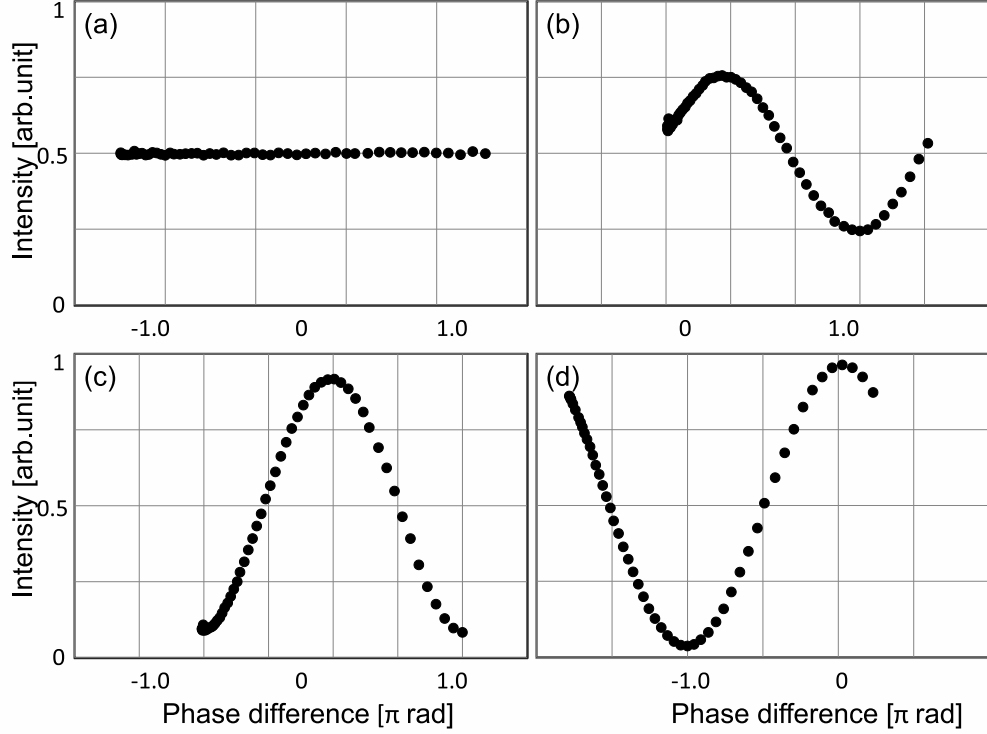


FIG. 5. Interference fringes for several values of the normalized minimum excitation: (a) $\Lambda = -1.6$, (b) $\Lambda = 0.074$, (c) $\Lambda = 0.49$, and (d) $\Lambda = 2.6$.

estimated visibility should have been overestimated. This overestimation causes no harm, from the conservative points of view for the security certification. However, it is undesirable for the practical use, because we may lose some amount of final key by unnecessary privacy amplification. The effect of the noise emerges significantly for small visibilities. To obtain better estimation, we examined the results showing low visibilities by magnifying the scale of intensity, as shown in Fig. 6. The error bars originated mainly from the noise of the sampling oscilloscope. The observed signal-to-noise ratio was about 17 dB, where the average intensity was normalized to 0.5. The r.m.s. value of the noise suggests that it may be hard to measure the visibility less than 0.02. Nevertheless, a periodic dependence on the phase difference is seen in Fig. 6 (b). By taking the center values denoted by squares in Fig. 6, we could fit the interference fringe with

$$I(\varphi) = A(1 + \Theta \cos(\varphi + \varphi_0)). \quad (17)$$

The result of the fitting is depicted as a thick solid line in Fig. 6. For excitation of $\Lambda = -1.6$ (a), the best fitting value for the visibility was 0.004, which reflected very weak periodic

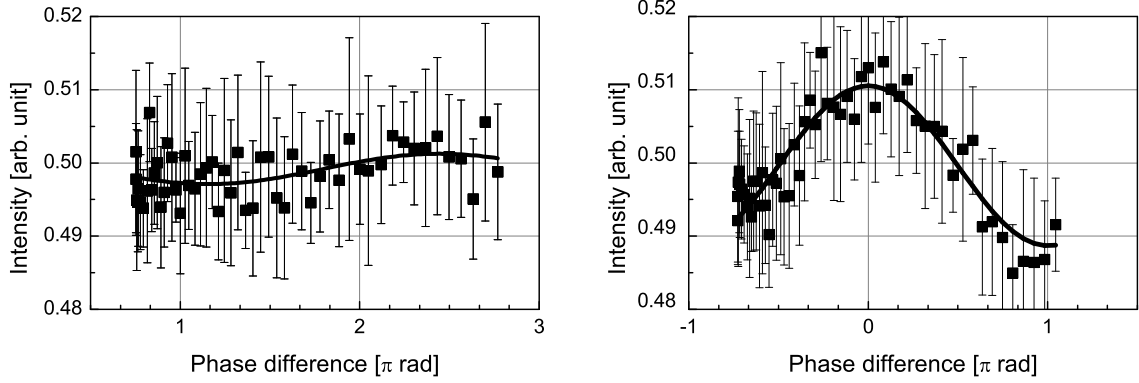


FIG. 6. Magnified view of the interference fringe. (a) $\Lambda = -1.6$ and (b) $\Lambda = -1.2$. Solid lines denote the fitted curve. The fitted values of the visibility were 0.004 and 0.02.

dependence on the phase difference. The fitted visibility was much less the one estimated from the maximum and minimum intensities, 0.014. For (b), $\Lambda = -1.2$, the fitted value of the visibility was 0.022, while the estimated one was 0.030. The fit was done well, as we consider the 95 % confidence interval of the fitting value [0.019, 0.025]. Discrepancy between the fitted and estimated visibility decreases as the visibility increases. On the basis of the above, we conclude that the present experimental set up can detect the visibility down to 0.02. The effect of the noise should be reduced by using low noise front-end and by increasing number of accumulation to obtain lower measurement limit of the visibility.

We applied the corrections discussed above. The results are summarized in Fig. 7, where the visibility is plotted as a function of the normalized minimum excitation. Figure 7 shows the visibility increases as the minimum excitation. It raises steeply around $\Lambda = 0$, where the LD was always turned on. The interference fringe almost disappeared when $\Lambda < -1$, i.e., the LD was reversely biased at the bottom. In particular, for $\Lambda = -1.6$ ($I_{DC} = 30.95$ mA,) the visibility was fitted to 0.004, which satisfied the strictest criterion given in sec. II B. Though the fitted value may not be accurate as described above, the visibility satisfied the target values 0.015 for the imbalanced coin at $\mu = 0.01$, and 0.044 for the decoy state discrimination. It should be noted that the interference fringe was observed even when the LD was turned off during the pulse interval. When the minimum drive current was set in the range $-1 < \Lambda < 0$, the light source can be no longer regarded as a phase randomized in terms of the imbalance of the quantum coin. For example, the visibility reached 0.08 for

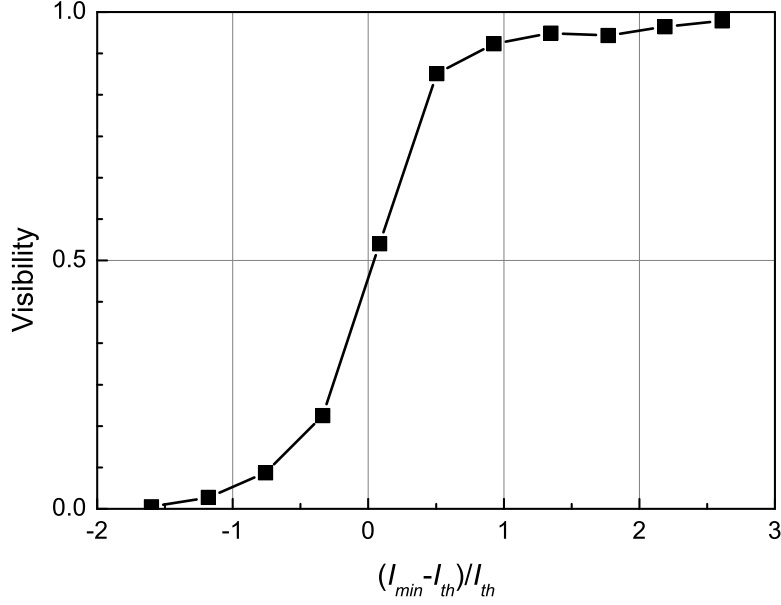


FIG. 7. Visibility of the interference as a function of the normalized minimum excitation Λ . For $\Lambda > 0$, the LD was always turned on. The LD was reversely biased at the bottom of the pulse, when $\Lambda < -1$.

$\Lambda = -0.76$. If we care only about the laser waveform (as is common in most applications,) we may set the bias to the value where the minimum drive current is close to the LD threshold, because it yields the best waveform as seen in Fig. 4 (b) and (c). Unfortunately, the phases of the pulses are correlated under this operating condition. The observed visibility was 0.534 for the case (c), where $\Lambda = 0.074$. The corresponding standard deviation of the phase distribution is about $\sigma = 1.12$. We need to scarify more bits to guarantee the security of final key in the privacy amplification under this operating condition.

In the following, we consider the dependence of the phase correlation on the minimum excitation in terms of effective photon life time. As described before, if the photons survive during the pulse interval, the phase may correlate with the previous pulses. Typical photon life time τ_{ph} of a LD cavity is several picoseconds. The effective photon lifetime can be increased by stimulated emission, even when the excitation is insufficient for lasing. Photon density S in the cavity will decay approximately as

$$\frac{dS}{dt} = \left(\Gamma g(n) - \frac{1}{\tau_{ph}} \right) S + n_{sp}, \quad (18)$$

where $\Gamma g(n)$ denotes the modal gain for the lasing mode at the carrier density n . The term n_{sp} represents the contribution of the spontaneous emission to the lasing mode. The photon field is governed by the spontaneous emission, when the photon density decreases to satisfy $S \leq n_{sp}$. Then, the phase of the light field become random.

The details of the dynamics is described with involved nonlinear coupled equations on photon density and carrier density. Roughly speaking, though, the photon field loses the phase information after the effective photon life time given by $-(\Gamma g(n) - 1/\tau_{ph})^{-1}$, as seen in Eq. (18). Since $(\Gamma g(n) - 1/\tau_{ph})\tau_{ph}$ equals approximately to $(I - I_{th})/I_{th}$, the effective photon lifetime scales with the inverse of the normalized excitation. When the normalized minimum excitation Λ exceeds zero, the effective photon life time becomes infinite to negative. Then, the photons of previous pulses remain to contribute the phase correlation. Even when Λ is less than zero, the photons may survive during the interval and contribute to the next lasing. For example, at $\Lambda = -0.33$, the effective photon the time life is about three times as large as the cavity life time at the bottom of the pulse. If we take the cavity life time as $\tau_{ph} = 3$ ps, the effective photon lifetime increases to 10 ps. This value is comparable to the turn-off duration of 13 ps calculated from Eq.(15). Therefore, a non-negligible number of photons are supposed to remain under this condition. In fact, the observed visibility was 0.188, indicating some phase correlation. For small excitation satisfying $\Lambda < -1$, the LD is reversely biased, and the effective photon life time should be equal to the cavity life time at least in the bottom of excitation. The calculated turn-off duration is as long as 30 ps for $\Lambda = -1.6$. Under this condition, photons should have disappeared during the pulse interval, and the lasing phase became random, as was observed in the experiment.

We see that observed dependence of the visibility on the excitation can be explained with the relation between the effective photon life time and the turn-off duration. A guide of the operating condition can be summarized that the effective photon lifetime should be less than the turn-off duration. As described above, this condition is satisfied with $\Lambda < -1$.

V. CONCLUSION

In BB84 protocol using an attenuated laser source, the secure key generation rate is lowered if the source emits non-phase randomized optical pulses. We evaluated the effect of the phase correlation in terms of the imbalance of the quantum coin and the discrimination

of the decoy from the signal pulses, for the partially coherent states. We obtained criteria for the source to be regarded as phase randomized. The target values for the visibilities were 0.006 and 0.015 in terms of the imbalance of the quantum coin at $\mu = 0.09$ and at $\mu = 0.01$, and 0.044 in terms of discrimination of the decoy pulses ($\nu = 0.1$) from the signal ($\mu = 0.5$.) We constructed a phase correlation test system to measure visibility of the interference fringe between the adjacent pulses using an asymmetric Mach-Zehnder interferometer. It enables to evaluate the phase correlation between the laser pulses experimentally at a high clock frequency of 10 GHz. We found that the phase correlation of the pulses from a LD depends on the operating condition. The target values were satisfied with the gain-switched LD. The operating condition is that the LD should be reversely biased at the bottom of the pulses, and the turn-off duration should be longer than the effective photon lifetime. The results indicate that QKD system clock can be increased to 10-GHz as far as the security issue on the laser light source is concerned. In practice, a number of technical problems remain. Among the remaining issues, the most important ones would be high speed photon detection and post-processing.

ACKNOWLEDGMENTS

The authors would like to thank Dr. Kiyoshi Tamaki and Dr. Yoshihiro Nambu for helpful discussions, and Mr. Takahisa Seki for his assistance in the experiment. This work has been conducted under the commissioned research of National Institute of Information and Communication Technology (NICT,) "Secure photonic network technology."

Appendix A: Optimal discrimination of two density matrices

We here derive the optimum discrimination of the decoy from the signal in partially coherent states, which were given in Eq. (14). We optimized the POVM for given values of P_{inc} to obtain the highest P_C in discriminating the two mixed states. All the density matrices here are real and symmetric. The POVMs Π_i , $i = 0, 1, 2$ satisfy

$$\Pi_0 + \Pi_1 + \Pi_2 = 1, \tag{A1}$$

where Π_1 and Π_2 correspond to the conclusive decision that the state is ρ_1 and ρ_2 , respectively, while Π_0 represents the inconclusive results. The probability of inconclusive results

is given by

$$P_{inc} = \text{Tr}(\rho \Pi_0) = 1 - \text{Tr}(\rho(\Pi_1 + \Pi_2)), \quad (\text{A2})$$

and the probability to yield a correct decision is

$$\begin{aligned} P_C &= p \text{Tr}(\rho_1 \Pi_1) + (1 - p) \text{Tr}(\rho_2 \Pi_2) \\ &= 1 - P_{inc} - p \text{Tr}(\rho_1 \Pi_2) - (1 - p) \text{Tr}(\rho_2 \Pi_1), \end{aligned} \quad (\text{A3})$$

where ρ is defined with the probability of ρ_1 's occurrence p by

$$\rho = p\rho_1 + (1 - p)\rho_2. \quad (\text{A4})$$

We applied the iteration method developed by Fiurášek and Ježek [27] to maximize P_C (A3) under the constraints (A1) and (A2) for a given value of P_{inc} using Lagrange multipliers. The iteration was performed with symmetrized equations to keep the POVMs Hermite and positive semi-definite. We set average photon numbers for the signal and decoy state $\mu = 0.5$ and $\nu = 0.1$, respectively, and assumed the signal and decoy state appear with the same probability ($p = 1/2$) for simplicity. The optimization was done for two values of the probability of the inconclusive results: $P_{inc} = 0.983$, which refers to the probability of the inconclusive results in the USD measurement to weak coherent states of $\theta_0 = 0$, and $P_{inc} = 0.712$ of $\theta_0 = \pi$. No USD measurement for $\theta_0 = 0$ exists to satisfy $P_{inc} = 0.712$. Figure 8 shows the probability of correct decision as a function of the standard deviation of phase. Successful USD measurement ($P_C = 1$) is achieved for the coherent states ($\sigma = 0$.) The probabilities of correct decision decrease as the standard deviation of phase increasing. The probabilities converge to the values for completely phase randomized states, when σ exceeds about 2.5, which corresponds to the visibility of 0.044.

We observed that the numerical optimization under the condition of $P_{inc} = 0.712$ sometimes failed, in particular for large σ . It also returned the probability of correct decision lower than that for the phase randomized states. Small errors in matrix operations may result in such suboptimal results. Nevertheless, we found the optimized POVMs for large σ states were almost the same as those for the phase randomized states. The optimized POVM operators were almost diagonal in photon-number state basis. The outcome ρ_1 was obtained when the observed photon number was larger than a threshold, while the inconclusive result was obtained when it was smaller than the threshold. The given probability

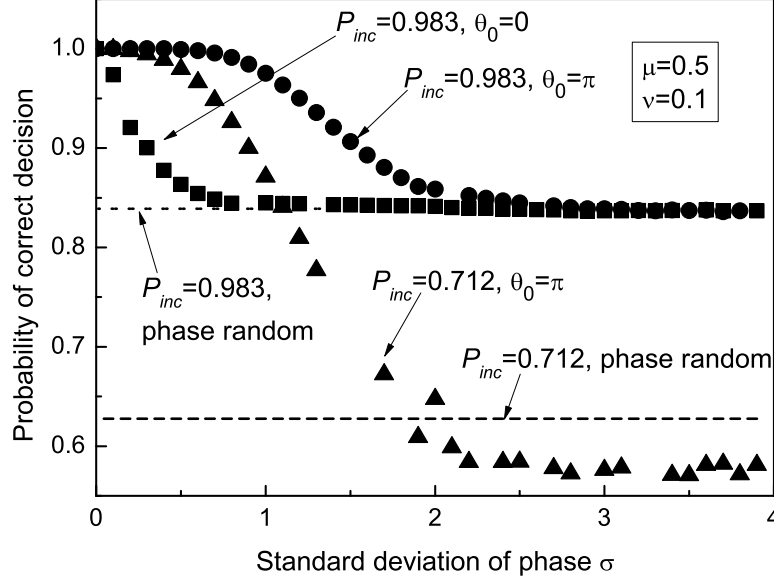


FIG. 8. Probability of correct decision as a function of the standard deviation of phase. State discrimination was done for the partially phase randomized states of average photon number 0.5 and 0.1. Squares represent $P_{inc} = 0.983$, $\theta_0 = 0$, circles $P_{inc} = 0.983$, $\theta_0 = \pi$, and triangles $P_{inc} = 0.712$, $\theta_0 = \pi$. Dotted line and dashed line refer to the probability of correct decision on the phase randomized states under the conditions of $P_{inc} = 0.983$ and $P_{inc} = 0.712$, respectively.

of the inconclusive results determined the threshold photon number.

-
- [1] C. H. Bennett and G. Brassard, in *Proc. IEEE International Conference on Computers, Systems, and Signal Processing* (1984) pp. 175–179.
 - [2] P. W. Shor and J. Preskill, *Phys. Rev. Lett.* **85**, 441 (2000).
 - [3] M. Koashi, arXiv: quant-ph/0505108v1 (2005).
 - [4] R. Renner, *Int. J. Quantum Info.* **6**, 1 (2008).
 - [5] M. Koashi, *New J. Phys.* **11**, 045018 (2009).
 - [6] M. Koashi and J. Preskill, *Phys Rev Lett* **90**, 057902 (2003).
 - [7] V. Scarani, H. Bechmann-Pasquinucci, N. J. Cerf, M. Dušek, N. Lütkenhaus, and M. Peev, *Rev. Mod. Phys.* **81**, 1301 (2009).

- [8] G. Brassard, N. Lütkenhaus, T. Mor, and B. C. Sanders, Phys. Rev. Lett. **85**, 1330 (2000).
- [9] D. Gottesman, H.-K. Lo, N. Lütkenhaus, and J. Preskill, Quantum Info. Comput. **4**, 325 (2004).
- [10] W.-Y. Hwang, Phys. Rev. Lett. **91**, 057901 (2003).
- [11] X.-B. Wang, Phys. Rev. Lett. **94**, 230503 (2005).
- [12] H.-K. Lo, X. Ma, and K. Chen, Phys. Rev. Lett. **94**, 230504 (2005).
- [13] M. Ben-Or, M. Horodecki, D. W. Leung, D. Mayers, and J. Oppenheim, in *Theory of Cryptography* (Springer, 2005) pp. 386–406.
- [14] J. Müller-Quade and R. Renner, New J. Phys. **11**, 085006 (2009).
- [15] M. Hayashi and T. Tsurumaru, New J. Phys. **14**, 093014 (2012).
- [16] M. Tomamichel, C. C. W. Lim, N. Gisin, and R. Renner, Nat. Commun. **3**, 634 (2012).
- [17] H.-K. Lo and J. Preskill, Quantum Info. Comput. **7**, 431 (2007).
- [18] Y.-L. Tang, H.-L. Yin, X. Ma, C.-H. F. Fung, Y. Liu, H.-L. Yong, T.-Y. Chen, C.-Z. Peng, Z.-B. Chen, and J.-W. Pan, Phys. Rev. A **88**, 022308 (2013).
- [19] Y. Zhao, B. Qi, and H.-K. Lo, Appl. Phys. Lett. **90**, 044106 (2007).
- [20] S.-H. Sun, M. Gao, M.-S. Jiang, C.-Y. Li, and L.-M. Liang, Phys. Rev. A **85**, 032304 (2012).
- [21] A. R. Dixon, Z. L. Yuan, J. F. Dynes, A. W. Sharpe, and A. J. Shields, Opt. Express **16**, 18790 (2008).
- [22] M. Sasaki, M. Fujiwara, H. Ishizuka, W. Klaus, K. Wakui, M. Takeoka, S. Miki, T. Yamashita, Z. Wang, A. Tanaka, K. Yoshino, Y. Nambu, S. Takahashi, A. Tajima, A. Tomita, T. Domeki, T. Hasegawa, Y. Sakai, H. Kobayashi, T. Asai, K. Shimizu, T. Tokura, T. Tsurumaru, M. Matsui, T. Honjo, K. Tamaki, H. Takesue, Y. Tokura, J. F. Dynes, A. R. Dixon, A. W. Sharpe, Z. L. Yuan, A. J. Shields, S. Uchikoga, M. Legré, S. Robyr, P. Trinkler, L. Monat, J.-B. Page, G. Ribordy, A. Poppe, A. Allacher, O. Maurhart, T. Länger, M. Peev, and A. Zeilinger, Opt. Express **19**, 10387 (2011).
- [23] K.-i. Yoshino, M. Fujiwara, A. Tanaka, S. Takahashi, A. Nambu, Yoshihiro and Tomita, S. Miki, T. Yamashita, Z. Wang, M. Sasaki, and A. Tajima, Opt. Lett. **37**, 223 (2012).
- [24] A. Yariv and P. Yeh, *Photonics*, 6th ed., The Oxford Series in Electrical and Computer Engineering (Oxford University Press, 2006).
- [25] C. H. Henry, IEEE J. Quantum Electron. **18**, 259 (1982).
- [26] K. Tamaki, M. Curty, G. Kato, H.-K. Lo, and K. Azuma, arXiv:1312.3514 [quant-ph] (2013).

[27] J. Fiurášek and M. Ježek, Phys. Rev. A **67**, 012321 (2003).